

**EXTRACTING SHORT-PERIOD SURFACE WAVEFORMS FROM SEISMIC NOISE FOR THE
PURPOSE OF ESTIMATING LOCAL AND NEAR-REGIONAL VELOCITY AND ATTENUATION
STRUCTURE**

Peter Gerstoft¹, William A Kuperman¹, Karim G. Sabra¹, Michael C Fehler², Steven R Taylor³,
and Toshiro Tanimoto⁴

University of California, San Diego¹, Los Alamos National Laboratory², Rocky Mountain Geophysics, LLC³,
and University of California, Santa Barbara⁴

Sponsored by Air Force Research Laboratory

Contract No. FA8718-07-C-0005¹⁻⁴

ABSTRACT

This paper investigates the utility of computing Time-Domain Green's Functions (TDGF) to be used for estimating velocity and attenuation structure for the purposes of nuclear explosion monitoring over local and near-regional distances. Our objective is to extend and apply the methodology of deriving TDGF for propagation between two receivers by cross correlation of seismic noise and/or coda of earthquakes observed at the receivers. We have previously shown that it is possible to obtain travel-time information for short-period surface waves (around 6 s) by cross correlating seismic noise at local and regional scales. The noise source exploited for this was the ever-present microseisms. In the present report, we focus on characterizing the spatiotemporal variation in microseisms from the Southern California seismic array.

OBJECTIVES

Our objective is to extend and apply the methodology of deriving TDGF for propagation between two receivers by cross-correlation of seismic noise and/or coda of earthquakes observed at the receivers. We have previously shown that it is possible to obtain travel-time information for short-period surface waves (around 6 s) by cross-correlating seismic noise at local and regional scales. We propose to add the following improvements to the TDGF method:

1) modifications to better handle cases having non-isotropic noise; 2) implementing a system identification approach for obtaining reliable amplitude information for the TDGF, allowing for the estimation of attenuation along paths between receivers, and 3) extracting TDGF from Lg or Sn coda.

In the present report, we focus on characterizing the azimuthal variation in microseisms from the Southern California seismic array. A non-uniform azimuthal distribution of energy might cause bias in travel times. The next objective will then be to demonstrate how much bias this will cause the extracted Greens functions and then use advanced beamforming approaches to correct for this bias.

RESEARCH ACCOMPLISHED

Introduction

Cross-correlation of noise recordings has been demonstrated to be a way to infer the impulse response between receivers. Extensive work has been performed on this topic in the last few years in various fields of wave physics such as ultrasonics, underwater acoustics, and geophysics, with early demonstrations by Weaver and Lobkis, 2001, and Larose et al., 2004. Despite the very different scales involved in ultrasonics (wavelength \sim mm) compared to geophysics (wavelength \sim km), the basic physics of the process is the same. The impulse response between two receivers is the part of the noise that is coherent between the two points, even if, at first sight, it is deeply buried in local incoherent noise. After cross-correlating over a long time (for example, one month in Sabra et al., 2005b; Shapiro et al., 2005), the time derivative of the noise cross-correlation function (DCF) converges to the impulse response between the two receivers filtered in the bandwidth of the noise spectrum.

A main issue in the convergence of the correlation process resides in the temporal and spatial distribution of the noise sources. From the temporal point of view, the noise spectrum defines the bandwidth frequency in which the impulse response will be retrieved. When receivers are far away from each other, the amplitude sensitivity of the receivers has to be such that the coherent propagating noise can be recorded on both receivers despite geometrical spreading and attenuation. This explains why only the slowly attenuated Rayleigh waves have dominated the results obtained so far from correlation of seismic noise. Using data recorded on a dense seismic network in Parkfield, California, we have successfully demonstrated that body waves can be retrieved (Roux et al., 2005b). The spatial distribution of seismic noise is also of importance. When noise sources are uniformly distributed on both sides of the receivers, the correlation function is symmetric in time, showing both the impulse response and its time-reversed signal (Snieder, 2004; Roux et al., 2005a; Sabra et al., 2005a). However, recent investigations using noise data recorded in Southern California did not result in a symmetric noise correlation function (NCF) because the noise was dominated by microseism originating from the ocean (Sabra et al., 2005a; Shapiro et al., 2005; Gerstoft et al., 2006b).

Noise Cross-Correlation and the TGDF

The cross-correlation C_{ij} is computed from the observed fields $v_i(\mathbf{r}_1, t)$ located at \mathbf{r}_1 recording component i and $v_j(\mathbf{r}_2, t)$ located at \mathbf{r}_2 recording component j by integration over the observation period T

$$C_{ij}(1, 2, t) = \int_0^T v_i(\mathbf{r}_1, \tau) v_j(\mathbf{r}_2, t - \tau) d\tau \quad (1)$$

In practice, the cross-correlation is computed for each day and then ensemble averaged over all observed days.

Analytic derivations for specific propagation models (Snieder, 2004; Roux et al., 2005a; Sabra et al., 2005a) and discussions in (Weaver and Lobkis, 2001; Weaver and Lobkis, 2004) give the following relationship between the

time-derivative of the noise cross-correlation $C_{ij}(1,2,t)$ between two seismic stations 1 (located at \mathbf{r}_1 recording component i) and 2 (located at \mathbf{r}_2 recording component j) for the TDGF $G_{ij}(\mathbf{r}_1; \mathbf{r}_2, t)$

$$\frac{dC}{dt} \approx -G_{ij}(\mathbf{r}_1; \mathbf{r}_2, t) + G_{ij}(\mathbf{r}_1; \mathbf{r}_2, -t) \quad (2)$$

The TDGF $G_{ij}(\mathbf{r}_1; \mathbf{r}_2, t)$ relates a unit force in direction i at \mathbf{r}_1 to the displacement response in direction j at \mathbf{r}_2 .

In Equation (1), the terms on the right-hand side are respectively: (1) the TDGF that comes from noise events that propagate from station 1 to 2 and yields a positive-correlation time-delay t and (2) the time-reversed TDGF which comes from noise events that propagate from station 2 to 1 and yields a negative correlation time-delay $-t$. Thus, for a uniform noise source distribution surrounding the two stations, the derivative of the DCF will be a symmetric function with respect to the arrival time because seismic noise sources are distributed on both sides of the station pair. However, in the case of a predominant directional noise source (e.g., noise originating from ocean microseisms, see next section), the DCF will likely be one-sided.

The DCF depends on the noise-spatial distribution and previous theoretical formulations assume an isotropic distribution. However, it can be argued qualitatively that if the noise field were dominated by a one-sided noise distribution, the DCF would have a shape as suggested in trace “B” of Figure 1b. This might represent the case of seismic noise dominated by microseisms (Sabra et al., 2005b; Shapiro et al., 2005). Another important case is a noise field that has two uncorrelated propagating components, e.g., seismic noise propagating as surface waves and body waves. The DCF would then have a shape as shown in trace “A” in Figure 1b.

Removal/Reduction of Noise Directionality

The seismic noise field is typically not isotropic and is dominated by noise sources having some preferred direction from a region, such as ocean microseisms (Bromirsky and Duennebie, 2002). Then, the station pair orientation will influence the quality of the TDGF that can be obtained from noise correlation. This yields one-sided arrival-time structure for the DCF. It can also cause a bias in travel-time estimation between the station pairs if the waves are not incoming near the station-pair axis (Gerstoft et al., 2006a). For example, if the noise source signal propagates mainly at an angle of 45 deg with respect to station pair axis, the resulting arrival DCF would overestimate the actual wave velocity by a factor of $\sqrt{2}$.

To first order for a weakly scattering medium (e.g., the Earth’s crust but not a random cavity), the regions of constructive interference for the noise sources contributing to the time-averaged DCF are roughly located in the two broad end-fire beams (Snieder, 2004; Roux et al., 2004; Sabra et al., 2005a). Noise sources located outside of these end-fire beams typically have a weaker contribution to the DCF. Thus, for a weakly scattering medium and anisotropic noise source distribution, coherent waveforms may not emerge easily from the DCF if the station pair is oriented roughly perpendicular to the main propagation path of the noise sources.

In order to obtain unbiased TDGF, it is preferable to have noise coming from all directions (Wapenaar, 2004). In practice, the noise is strongly directional, but even then, it is still possible to obtain reasonable estimates of the arrival time. These will likely be biased, and we expect that the amplitude of the arrival is more sensitive to a nonuniform distribution of the noise. In principle, by beamforming it should be possible to eliminate certain directions and/or enhance arrivals from other directions. The approach would then be transforming the noise to the two-dimensional (2-D) slowness domain, filtering, and then transforming the slowness spectrum back to the time domain. As long as the propagating noise level is above the nonpropagating noise level, we expect such a transformation to be feasible. Three related filtering approaches are a) removal of noise propagating in certain directions, b) enhancing certain directions, and c) equalizing the directional noise arrival spectrum so that the noise arrives uniformly from all directions. Instead of forming a beam in the direction towards the noise source (Rost and Thomas, 2002), we will null steer on these sources, which actually is the complement of beamforming and a standard goal of adaptive array processing (e.g., Johnson and Dudgeon, 1993). The purpose of this is to eliminate signals from certain directions. Ideally, this would lead to spatial prewhitening of the signals. The spatial prewhitening should give good results as long as noise is propagating in all directions (it should not be a problem

that some directions have more energy). Spatially prewhitening the propagating noise field should result in more stable TDGF and unbiased travel times.

Seismic Noise Beamforming

Using continuous data recorded in the year 2006 on all the 155 seismic stations (vertical component with sampling rate 1 per second) in Southern California, we formed beams and determined the azimuth and slowness of the waves crossing the array as a function of frequency (Johnson and Dudgeon, 1993; Rost and Thomas, 2002). A similar processing was used for detecting Katrina in California (Gerstoft et al., 2006a) and proceeds as follows:

First, in the monthly time series, unwanted events (e.g., earthquakes) are removed by truncating signal amplitude above one standard deviation, calculated for the monthly time series. The data is split into 512-s time series, Fourier transformed, and corrected for instrument response. For each frequency, we only keep the phase of the signal. Amplitude information is lost here, but this will remove undesirable signals caused by local site amplification effects and local large noise event. This is also consistent with the simple plane wave model used in the processing. However, all frequencies will then have equal power, meaning that the typical microseism spectrum will not be retrieved if the resulting power spectrum is extracted. At each frequency, we have a complex-valued vector $\mathbf{v}(\omega, t_i)$ containing the response from the 155 stations, where t_i refers to the time of the Fourier transform.

The cross-spectral density matrix is then formed by ensemble averaging (\dagger denotes the transpose complex conjugate)

$$\mathbf{C}(\omega, t) = \sum_{n=1}^N \mathbf{v}(\omega, t + t_n) \dagger \mathbf{v}(\omega, t + t_n) \quad (3)$$

The i th row and j th column of \mathbf{C} contains the average phase delay between the i th and j th seismometer at frequency ω . In the time domain, this would correspond to the cross-correlation between the two seismometers.

For this study, we used $N=10$. This corresponds to an averaging time of 10×512 s or 1.5 hour, agreeing well with the minimum resolution time of weather systems. For a given frequency ω , phase slowness s , and azimuth θ , the plane wave response for the array of geophones is

$$\mathbf{p}(\omega, s, \theta, \mathbf{r}) = \exp(i\omega s \mathbf{r} \mathbf{e}) \quad (4)$$

where $\mathbf{e} = (\sin \theta, \cos \theta)$ is the directional cosines and \mathbf{r} is the coordinates of the geophones with respect to their mean. The beamforming output is then given by

$$b(\omega, s, \theta, t) = \mathbf{p} \dagger(\omega, s, \theta, \mathbf{r}) \mathbf{C}(\omega, t) \mathbf{p}(\omega, s, \theta, \mathbf{r}) \quad (5)$$

Processing a whole year of data gives a four-dimensional (4-D) matrix containing the beamformer output as a function of time, frequency, angle, and slowness. There is no averaging across frequency giving a frequency resolution of $1/512 = 0.002$ Hz. Based on a plane wave simulation, for a 0.1-Hz frequency and phase speed of 3 km/s, the array 3-dB beamwidth was 4° . Inhomogeneous velocity structure and array bias may cause a further smearing out of the peaks.

For each frequency analyzed, we searched for the combination of phase slowness and azimuth that gave the best fit to the data. Based on these phase slownesses, it was observed that they are independent of both time and azimuth and showed the Rayleigh wave dispersion with frequency $s = s(\omega)$, similar to the results in Gerstoft et al., 2006a. The dispersion can be determined by averaging over time and azimuth. Thus, the beamformer output only depends on $b(\omega, s, \theta, t)$.

Beamformer Output

The beamformer output is shown in Figure 2 at three frequencies 0.07 Hz (primary microseisms), 0.12, and 0.14 Hz (secondary microseism) for the whole month of January and July 2006.

In January, a string of storms (Bancroft, 2006) hit the Vancouver Island/Oregon area. The seismic noise from most of these storms was detected by the Southern California array. An example of such a storm is shown in Figure 3 for 2100 UTC Jan 8, both for the significant wave height and the dominant peak frequency (Tolman, 2005). In the beamformer output (Figures 2a and 2b) the primary microseisms (0.07 Hz) can clearly be seen for azimuths from 310–340° consistent with a source region in the coastal areas of the N Pacific. After the ocean waves hit the Northern Pacific Coast, ocean waves for the same storm arrives in Southern California/Baja California area about a day later (excellent hindcast videos demonstrate this [Tolman, 2005]). This can be seen in Figure 2a as striations from about 300° to 160° for all three frequencies. For most of the storms the primary microseisms give a strong response at 160° corresponding to a source region near the coast of Baja California.

Strong microseisms can be seen from azimuth 40–60° corresponding to a source region in the Northwest Atlantic. The microseisms also correlate well with the storm activity in the Labrador Sea/Northwest Atlantic (Bancroft, 2006). Most of these storms are not easily identifiable in the secondary microseism bands (Figure 3a), although later discussion shows primary and secondary microseisms.

For the secondary microseisms (0.12 and 0.14 Hz in Figure 2a), a broad azimuth range from about 160-320° is fairly uniformly activated. This indicates a different source mechanism for the secondary microseisms, as has been advocated by interaction of opposing wave trains. A weak response can also be seen at azimuth 140°. This corresponds to microseisms from the Gulf of California. One reason that the primary microseisms are stronger in azimuth 300-340° and the secondary microseisms are weaker in that azimuth may be because of higher attenuation for high-frequency waves including both scattering and intrinsic attenuation.

In July, the North Pacific is relatively calm, and the primary microseisms mainly come from a constant azimuth about 210°. This constant direction does not mean that all storms come from this direction as these waves have been refracted near the coast and propagate perpendicular to the coast. The secondary microseisms are seen from a wider azimuth from 170–270°, again indicating a difference in excitation mechanism.

Whole Year

A good overview of the microseisms activity can be obtained by examining the azimuth corresponding to the maximum beamformer output. Figure 4 shows variations in azimuth for the whole year in the frequency interval 0.04-0.18 Hz. The main feature is that in the winter months most peak azimuths come from NW (hereafter we use abbreviations for azimuth, N, S, E, and W), whereas in the summer months they come from SSW.

The signature for each storm emerges in this figure as striations, as higher frequencies arrive later. This feature can be explained from the dispersion of the ocean waves (Haubrich et al., 1963) and gives us a clue on distance to the storms. In deep water, the ocean-wave group speed at frequency f is given by

$$c_g = \frac{g}{4\pi f} \quad (6)$$

Since propagation of ocean waves in the frequency range 0.04-0.18 Hz can be regarded as those of deep-water waves, if the distance from a storm is R , the arrival time is given as $T = R / c_g = 4\pi f R / g$. From the arrival azimuth versus frequency and time, we can measure the slope $\frac{dT}{df}$, and this gives the distance to the storm

$$R = \frac{dT}{df} \frac{g}{4\pi} \quad (7)$$

This can be used to determine the distance to the storm if all waves are recorded at the same point. The storms in January (Figure 4) have a slope of 40 days/Hz typically, giving a distance to the storm of 4000 km. This corresponds to the storms originating in the NE Pacific. This can be confirmed by watching the hindcasts (Tolman, 2005). In November and December, the N Pacific storms originate in the NW Pacific and thus the distance to the coast is

considerably less, resulting in a small slope. In the winter (November–February), it is observed that peak azimuth of the primary microseisms comes from NW, but the secondary comes from about W, thus the generation of the microseisms is not at the same point. This will cause a bias in the estimated distances above but the above formula can still be used for a rough estimate.

A few storms in June–September have a steeper slope of 80 days/Hz, giving a distance to the storm of 8000 km. This corresponds to storms in the South Pacific and is in agreement with the hindcasts (see videos [Tolman, 2005]) and previous observations (Haubrich et al., 1963). The fact that we can observe the striations of most storms indicates that the ocean waves have propagated a long distance before coupling into seismic energy. This implies that a major part of the microseisms has been generated along the Pacific Coast. The linear signature of the storms can be observed in the secondary microseisms band in Figure 4. This is due to the dispersive nature of the ocean waves, and thus a part of the energy in the secondary microseism band is generated by direct interaction with the ocean wave. In general, the secondary microseism is distributed over a large azimuth, 90–180° (Figure 4).

Spectral low amplitudes are seen between the primary and secondary microseisms (typically, 0.08–0.1 Hz), and it is often possible to observe distant events. In September, signals for tropical storm Ernesto (1–3 Sep) and Hurricanes Florence (11–13 Sep) and Helene (25–29 Sep), can be observed. Tropical storm Ernesto was the weakest and made landfall at 4 am UTC 1 September in North Carolina. Microseisms can first be observed a day later from the coast of Georgia (dashed lines in Figure 5a). About 1–1.5 days after landfall, microseisms from the coast of Virginia are observed (solid lines in Figure 5a).

In the summer and fall, noise from NE occurs mostly in the 0.1 Hz spectral low where there is not much power from the Pacific Ocean waves. The origin of this noise is not clear since it do not correlate with major storms (Bancroft, 2006). Several storms from the Lawrence Sea can be observed in February and March in the primary and secondary microseism bands. According to the Mariners Weather Log (Bancroft, 2006), the western North Atlantic storm of February 22 to March 1 developed hurricane force winds. It can be observed with azimuths from 36–50° corresponding to the extent of the northeast coast of the Labrador Peninsula; see Figure 5b. Schulte-Pelkum et al. (2004) also observed microseisms in California from the Labrador Sea. Note, that land fast sea ice covers the NE coast of Labrador Peninsula in the winter. Other storms described in the Mariners Weather Log can also be observed: the North Atlantic storm of February 10–14 and the western Atlantic storm of March 26–28. Note, that the two western Atlantic storms generate strongly localized secondary microseisms.

CONCLUSIONS AND RECOMMENDATIONS

Microseisms are often the propagating background noise exploited when extracting the impulse response from noise. Thus, it is important to understand their origin and spatiotemporal distribution. When extracting the impulse response from noise, azimuthal variations can cause biases in the extracted impulse response, and this will also cause an unknown bias in the tomographic surface velocity. If the azimuthal variation in the microseisms is known, we might potentially be able to correct for this bias in the resulting estimate of the impulse response. In the present report, we are mainly concerned with describing the variation. Frequency domain beamforming using distributed arrays provides a powerful tool to monitor microseisms.

Microseisms were examined for a whole year with their daily and seasonal variations. From this it is clear that most of the microseisms are generated near the coasts. Distance to the storms can be estimated approximately, using the gradient of striation in the azimuth vs. frequency plot. In winter, the primary microseisms are dominated by excitation in northwest direction, thus, the North Pacific, but some significant excitation is occurring also in the North Atlantic. Much smaller excitations are also seen off the coast of Southern California. In summer, the azimuth of excitation is about 210° suggesting excitation near the coastal area of Southern California and mainly by ocean waves shoaling in the perpendicular direction to the coast. Excitation of the secondary microseisms occurs over wider azimuth from about 180–320° throughout the year, although the azimuth range is wider in winter. Differences in excitation mechanisms between the primary and secondary microseisms are thus obvious from beamforming results.

REFERENCES

- Bancroft, G. P., Mariners Weather Log, National Weather Service (NWS), <http://www.vos.noaa.gov/mwl.shtml>.
- Bromirsky, P. D., and F. K. Duennebieber (2002). The near-coastal microseism spectrum: spatial and temporal wave climate relationships, *J. Geophys. Res.* 107: (B8), 2166, doi:10.1029/2001JB000265.
- Gerstoft, P., MC Fehler, and KG Sabra (2006a). When Katrina hit California, *Geophys. Res. Lett.* 33: L17308, doi:10.1029/2006GL027270.
- Gerstoft, P., K. G. Sabra, P. Roux, W. A. Kuperman, and M. C. Fehler (2006b). Green's functions extraction and surface-wave tomography from microseisms in southern California, *Geophysics* 71: S123–S131.
- Johnson, D. H. and D. E. Dudgeon (1993). *Array Signal Processing: Concepts and Techniques*, Prentice-Hall.
- Larose E., A. Derode, M. Campillo, and M. Fink (2004). Imaging from one-bit correlations of wideband diffuse wavefields, *J. Appl. Phys* 95: 8393–8399.
- Rost, S., and C. Thomas (2002). Array seismology: methods and applications, *Reviews of geophysics* 40: doi:20.1029/200RG000100.
- Roux, P., K.G. Sabra, W.A. Kuperman and A. Roux (2005a). Ambient noise cross-correlation in free space: theoretical approach, *J. Acoust. Soc. Am.* 117: 79–84.
- Roux, P., K. G. Sabra, P. Gerstoft, W.A. Kuperman, and M. Fehler (2005b). P-waves from cross-correlation of seismic noise, *Geophys. Res. Lett.* 32: L19303, doi:10.1029/2005GL023803.
- Sabra, K. G., P. Gerstoft, P. Roux, W.A. Kuperman, and M. C. Fehler (2005a). Extracting time-domain Greens function estimates from ambient seismic noise, *Geophys. Res. Lett.* 32: L03310.
- Sabra, K., P. Gerstoft, P Roux, W.A. Kuperman, M. Fehler (2005b). Surface wave tomography from microseisms in Southern California, *AGU Geophys. Res. Lett.* 32: L14311, doi:10.1029/2005GL023155.
- Shapiro, N. M., M. Campillo, L. Stehly and M.H. Ritzwoller (2005). High-resolution surface-wave tomography from ambient seismic noise, *Science* 29: 1615–1617.
- Schulte-Pelkum, V., P. S. Earle, F. L. Vernon (2004). strong directivity of ocean-generated seismic noise, *Geochem. Geophys. Geosyst.* 5: 10.1029/2003GC000520.
- Snieder, R. (2004). Extracting the Green s function from the correlation of coda waves: A derivation based on stationary phase, *Physical Review E* 69: 046610.
- Tolman, H. L. (2005). Manual and Wave User system documentation of WAVEWATCH-III version 2.22, US Depart. of Commerce. Hindcast files available from <http://polar.ncep.noaa.gov>.
- Wapenaar, K. (2004). Retrieving the Elastodynamic Green's Function of an Arbitrary Inhomogeneous Medium by Cross Correlation, *Phys. Rev. Lett* 93: 254301.
- Weaver, R. L., and O.I. Lobkis (2001). Ultrasonics without a source: thermal fluctuation correlations at MHz Frequencies, *Phys. Rev. Lett.* 87: 134301.
- Weaver, R. L., and O. I. Lobkis (2004). Diffuse fields in open systems and the emergence of the Green's function, *J. Acoust. Soc. Am.* 116: 2731–2734.

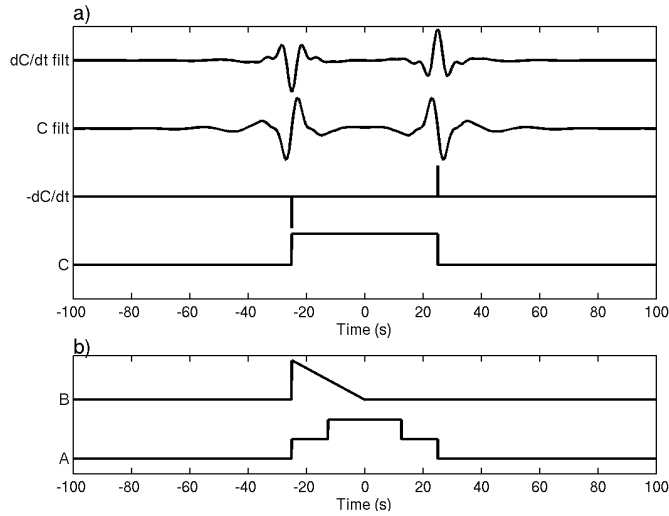


Figure 1. a) Schematic of the measured cross-correlation function and its time-derivative for an isotropic distribution of random impulse sources for infinite bandwidth or for a finite bandwidth (0.05–0.2 Hz). b) Influence of the noise source spatial distribution and origin. Trace B: A single-sided noise source distribution yields a one-sided noise cross-correlation function. Trace A: Cross-correlation function of a noise field having two propagating components with different velocities and amplitudes.

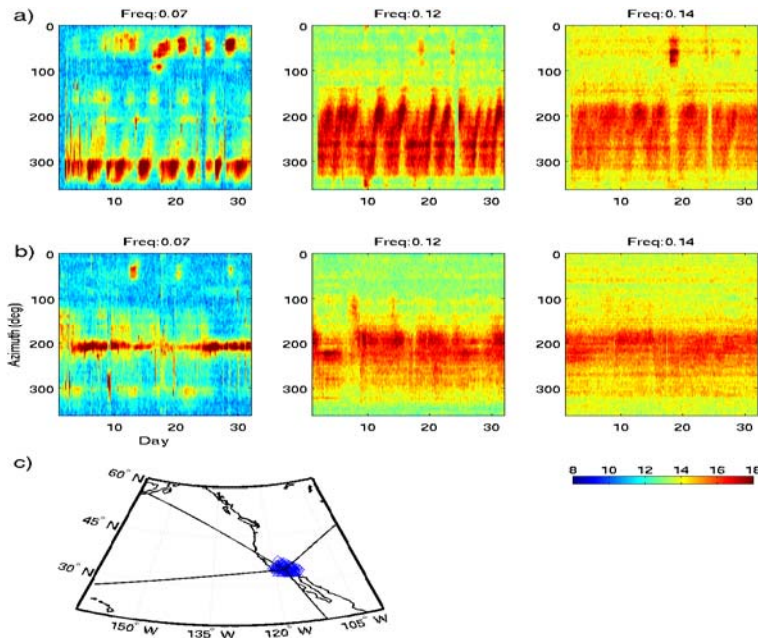


Figure 2. Beamformer output versus azimuth and days in month for frequencies 0.7, 0.12, and 0.14 Hz during a) January and b) July 2006. c) Map of region, showing stations in Southern California and important azimuths from the array: 45°, 150°, 270°, and 320°.

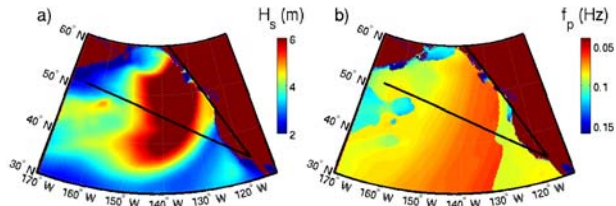


Figure 3. January storm in the North Pacific. In January a string of storms originating from the NE Pacific hit the Pacific coast, here shown for 8 January 21:00 UTC, showing a) significant wave height and b) peak frequency. Azimuths 310° and 340° are indicated.

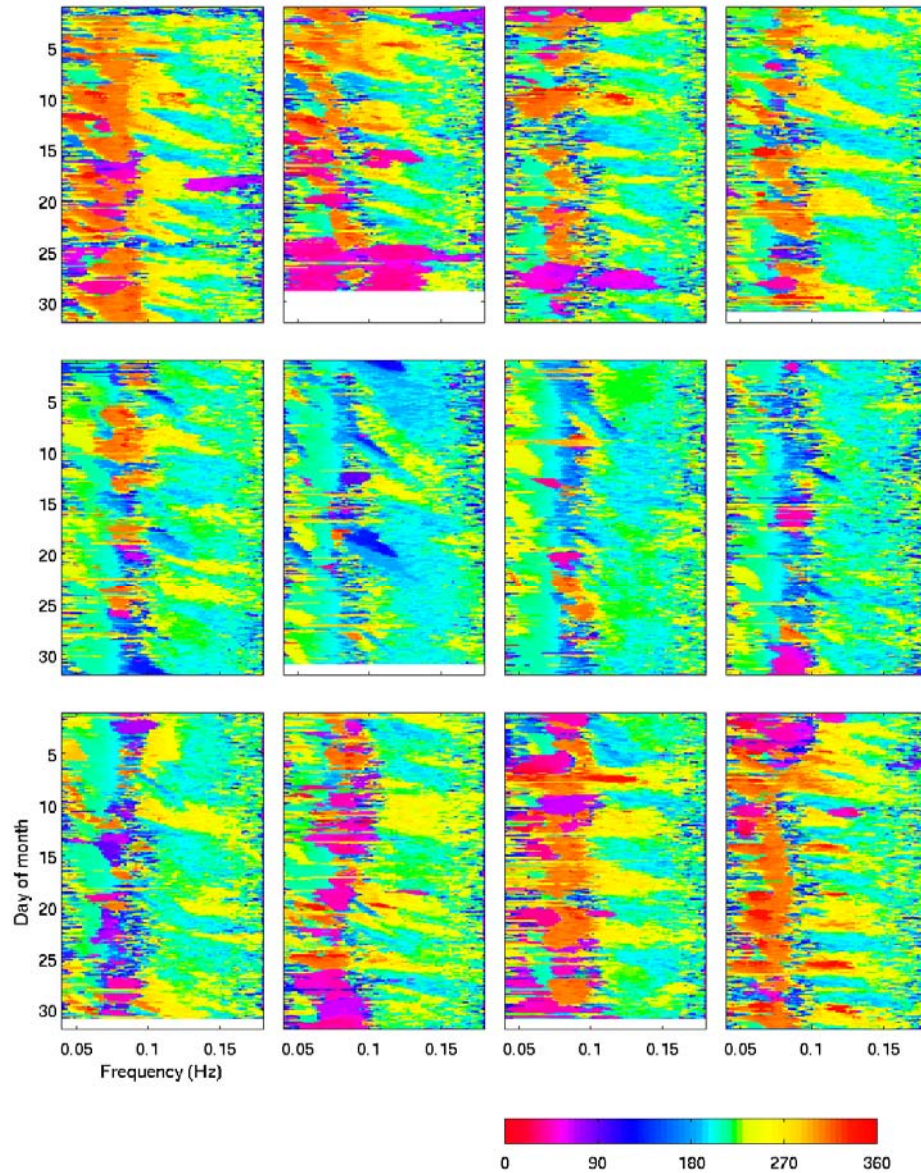


Figure 4. Azimuth (deg) from whole array for each month of 2006. Each subplot corresponds to one month.

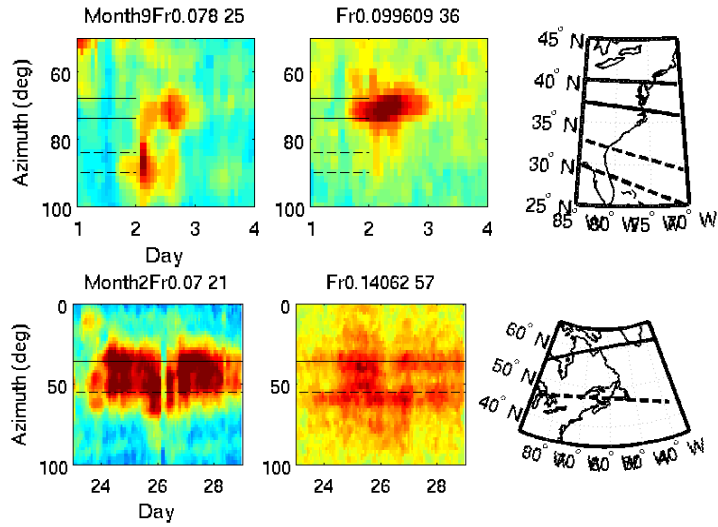


Figure 5. Beamformer output for two storms in the Atlantic. a) Tropical storm Ernesto 1–3 September at frequency 0.08 and 0.1 Hz and corresponding map. b) North Atlantic storm of 24 February to 1 March at frequency 0.7 and 1.4 Hz. The azimuths corresponding to the NE of the Newfoundland/Labrador Peninsula is shown in the map.